0163–4984/96/3602–3–0093 $13.75

Nanoscale Iron Crystallites Encapsulated in Nonmagnetic Metal Shells

Synthesis, Chemical, and Magnetic Properties of Core/Shell Iron-Indium, Iron-Neodymium, and Related Materials

DAJIE ZHANG,[1] GEORGE GLAVEE,[1]
KENNETH J. KLABUNDE,[1]* GEORGE C. HADJIPANAYIS,[2]
AND CHRISTOPHER M. SORENSEN[1]

[1]*Departments of Chemistry and Physics, Kansas State University, Manhattan, KS 66506;*
[2]*Department of Physics, University of Delaware, Newark, DE 19716*

Accepted September 15, 1996

ABSTRACT

Further work is reported on the use of the Solvated-Metal-Atom-Dispersion (SMAD) method for preparing metastable alloy nanoparticles of immiscible metals. On heat treatment, the nanoparticles phase separated; in the case of Fe-In and Fe-Nd, core/shell structures were formed with Fe as the core, but with Fe-Au, Fe-Bi, Fe-Ca, Co-Mg, and Ni-Mg, either stable alloys or segregated particles were formed. The core/shell particles were protected from environmental oxidation in part or completely, depending on the heat treatment temperatures (degree of phase separation). Magnetic studies of the [In]Fe and [Nd]Fe samples, after passivation, showed low coercivities, H_c, and Fe crystallite size-dependent saturation magnetization M_s. Although partial oxidation of the smaller Fe crystallites was a complicating feature, the data suggest that the In and Nd cause a dead-layer effect in which Fe atoms in contact with the In or Nd phase have their magnetic moments quenched. In the case of Fe-Nd, at the

*Author to whom all correspondence and reprint requests should be addressed.

highest heat-treatment temperature, an Fe_2Nd phase was also formed that further quenched M_s for the remaining iron core.

Index Entries: Iron; indium; neodymium; nanoparticles; core/shell; magnetism.

INTRODUCTION

A major driving force behind the study of nanoscale ferromagnetic particles is the search for better magnetic recording materials *(1–2)*. Important characteristics of a recording medium include the domain structure. Each particle should be a single domain unit that possesses two stable opposite magnetic poles along a preferred axis. The switching field is the minimum magnetic field needed to switch the magnetic poles in the single domain particles. The size of the switch units (single domain particles) is critical to the performance of the recording medium. They should be small enough to allow recording of the intended magnetization pattern and to provide a high signal-to-noise ratio, which requires the use of small switch units that are partially independent, so that one unit is not strongly affected by the magnetization of the other units *(3)*.

The important magnetic characteristics of the particles include the saturation magnetization, M_s, remnant magnetization, M_r, and coercivity, H_c *(3)* M_r is important because it is the maximum magnetization intensity that the material can retain, and M_r depends on M_s as well as how the preferred axes of the domains are aligned with the direction of the external magnetic field. The value of H_c (an extrinsic property) represents the difficulty of achieving magnetic reversal, and must be adjusted for desired magnetic recording, writing, and erasing.

A magnetic recording medium must be chemically stable under the conditions employed. For this reason, metallic Fe, Co, or Ni, being extremely oxophilic in ultrafine particle form, are generally not useful. Instead, iron oxide, chromium oxide (CrO_2), Co^{2+}-enhanced iron oxide, and barium ferrite ($BaFe_2O_4$) are most common *(2)*.

High-density recording requires materials with high M_s, M_r, and H_c. All the aforementioned metal oxides have magnetization intensities M_s in the range of 300–400 emu/cm^3, which cannot meet the need. Therefore, metallic particles have attracted more and more attention in the development of high-density recording materials. For instance, iron metal has a magnetization intensity of 1700 emu/cm^3, which is several times that of γ-Fe_2O_3 or CrO_2. Also, oxide-coated Fe^0 particles have exhibited coercivities as high as 1000 Oe, suitable for high-density recording. The other ferromagnetic metals also show promise; i.e., Co^0 = 1430 emu/cm^3 and Ni^0 = 490 emu/cm^3.

Metal particles for magnetic recording have been prepared in a number of ways, including evaporation into gases *(4–7)*, borohydride reduction *(8,9)*, alkali metal reduction *(10,11)*, and many other clever

techniques *(12–14)*. However, such particles readily oxidize and often consist of 50–70% of oxides by volume, and then exhibit magnetization intensities of 700–900 emu/cm^3. Various methods have been employed to protect the metal particles, such as coating with polymers or surfactants *(15–17)*. Coevaporation or cosputtering with nonmagnetic materials have also met with some successes, such as Fe-Al_2O_3 *(18)* Fe-SiO_2, and Fe-BN (by using rf magnetron sputtering) *(19)* and Fe-Mg *(20)*. In this way granular solids are obtained with Fe nanoparticles contained within matrix hosts of Al_2O_3, SiO_2, or BN. Mechanical alloying, also called high-energy ball milling, is another method to force partial mixing of immiscible components. Examples include Fe-SiO_2 *(21)* and $Fe_{100-x}M_x$ (M = Al, Si, Cu) *(22)*. The Melt-Spun method has also been used, for which melts are rapidly quenched, forming ribbons of "alloys" of immiscible metals *(23–25)*. Heat treatment can later be applied to force some phase segregation and crystallite (grain) growth if desired.

THE SOLVATED-METAL-ATOM-DISPERSION (SMAD) *(26)* METHOD WITH IMMISCIBLE METALS

The challenge is to prepare protected nanoscale magnetic metal particles as free-flowing powders. One approach is to prepare metastable alloys as individual particles, which can be done by codepositing the vapors of the two immiscible metals into a low temperature "inert" matrix. On warming the matrix, isolated metal atoms must migrate and are forced, in a kinetic sense, to form metastable alloys, such as Fe and In as shown in Fig. 1. Preferably, the second metal must be more oxophilic than iron so that any trace of oxygen present is scavenged as another protecting mode. However, the second metal could be inert (e.g., Au), but in either case the eventual coating must be impermeable to oxygen or other environmental gases.

Earlier we reported some initial successes for this approach for Li and Mg-Fe pairs *(27,28)*. By examining the phase diagrams of Fe, Co, and Ni with a list of second metals, several other interesting systems were chosen, which include indium, calcium, gold, and neodymium, and the findings are reported herein.

EXPERIMENTAL APPROACH

Chemicals

1. Iron metal chips (Fisher Scientific, Fairlawn, NJ).
2. Magnesium metal rod (6 mm diameter), 99.9+% purity (Aldrich, Milwaukee, WI).
3. Indium metal rod (6 mm diameter), 99.9+% purity (Aldrich).

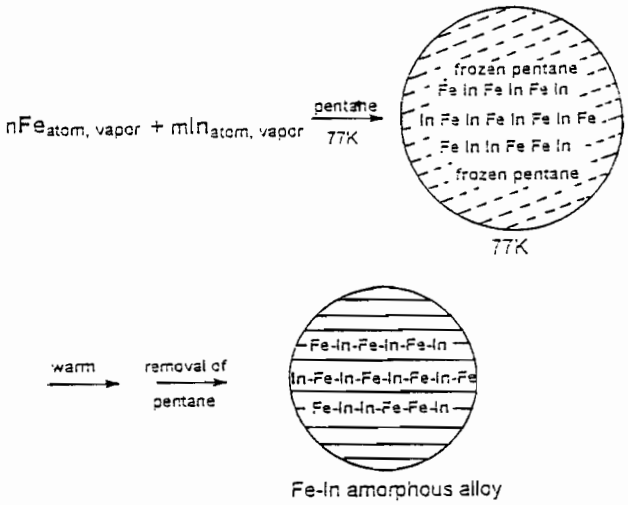

Fig. 1. The formation of amorphous Fe-In alloys in a SMAD reaction.

4. Cobalt metal pieces, 99.5% purity (Aldrich).
5. Neodymium ingot, 99.5% purity (Strem Chemicals, Newburyport, MA).
6. Canadian 50 g 24 karat gold coin.
7. *N*-pentane, HPLC grade, (Fisher Chemical/Fisher Scientific).

Pentane was predried by refluxing over Na/K with benzophenone. Before going to the SMAD reactor, the dried pentane held in a Schlenk tube was degassed on a vacuum line with liquid nitrogen. The crucibles used were tungsten baskets obtained from R. D. Mathis; they were coated with a water-based alumina cement (Zircar Alumina Cement) obtained from Zircar Products, Inc. The Zircar Alumina Cement consisted of 70% of alumina in a combination of milled fibers and submicroparticles. It is mildly acidic (pH 5.0) and forms a strong bond on removal of the water solvent. Prior to use, the coated crucibles were first heated at <100°C in air for 2 h, then heated to red-hot in vacuum at increments of about 200°C for 2 h at each temperature to eliminate the volatiles. This careful programming of heating temperatures also avoided the cracking of the alumina coating. The temperature limit of these crucibles is 1650°C.

EQUIPMENT

X-Ray Powder Diffraction: SCINTAG 3000 XRD Diffractometer

X-ray powder diffraction (XRD) was used to study the chemical compositions and structures of the powders. For samples with a fresh

surface, mineral oil was applied to coat the sample for temporary protection from oxidation by forming a powder/oil paste in an argon-filled drybox. Since the protection from mineral oil was found to be effective only for a few hours, XRD analysis (which takes about 1 h) was carried out immediately after the coating. For samples with passivated surfaces, no such precaution was taken. This does not suggest that such protection was unnecessary; XRD after exposure was one test of the effectiveness of the passivated surfaces.

X-ray powder diffraction is also a very useful tool for estimating the crystallite sizes of the metal particles. This can be achieved with the aid of the Scherrer formula:

$$t = 0.91\lambda/B\cos\theta_B \tag{1}$$

where λ is the X-ray wavelength, t is the crystallite diameter in Å, B is the width of the peak at half height, and θ_B is the half value of the peak position in degrees.

BET Surface Area: Micrometrics Flowsorb II 2300 BET

The direct information from a BET measurement is the surface area of the particles. Under assumed conditions, such as the particles being spherically shaped and individually spaced, the average size of the particles can be calculated from the specific surface area data. It can be shown as follows: Given a group of spherical particles N with the total mass of M, the average specific area of these particles is.

$$S = (N)\ (4\pi R^2)/M \tag{2}$$

where R is the average radius of these particles. Since M is equal to $N(4/3)\pi R^3\rho$, where ρ is the average density of the particles, therefore, the term $(4/3)\pi R^3\rho$ is the average mass of the particles. Finally, we have:

$$S = N(4\pi R^2)/N(4/3)\pi R^3\rho \tag{3}$$

$$S = 3/R\rho \tag{4}$$

and

$$R = 3/S\rho, \tag{5}$$

so the average BET size t of the particles is:

$$t = 2R = 6/S\rho. \tag{6}$$

Transmission Electron Microscopy (TEM)

Both the overall particle sizes and the Fe crystallite sizes could be estimated from TEM studies. A small amount of sample (3–5 mg) was

placed in a sample vial containing toluene; then, after being agitated for 3–5 min in a sonicator, a suspension of the particles was formed. One drop of the suspension was transferred onto a carbon-coated copper grid as the sample holder. After evaporation of the solvent, the sample was ready for TEM study. To avoid sintering of the particles caused by the heat generated by the electron beam, liquid nitrogen was used to cool the sample chamber during the study.

Mössbauer Spectroscopy

The Mössbauer spectra were obtained on a Ranger Scientific Inc. MS-1200 Mössbauer spectrometer. α-Fe was used as the standard. Mössbauer spectroscopy was used to study the oxidation states and the fine structures (e.g., Fe crystallite size, surface/interface effect on the Mössbauer parameters of iron) of iron species in the samples. Approximately 5–10 mg of elemental iron is required for the study. Thus, the amount of sample required in each study can be estimated based on the mass balance of the sample. Similar to the XRD studies, samples with fresh surfaces were protected with mineral oil before being transferred into the sample chamber. Mössbauer spectra could be taken at both room temperature (298K) and liquid nitrogen temperature (77K).

SQUID Magnetometry

Magnetic properties of the samples were taken from a MPMS2 (Magnetic Property Measurement System) SQUID (Superconducting Quantum Interference Device) magnetometer designed by Quantum Design. The field range of the equipment is ±55,000 Oe, with a sensitivity of 10^{-8} emu. Fresh samples were protected in mineral oil in a gel capsule during the measurement. Magnetization curves of these samples were taken at different temperatures between 10 and 300K in fields up to 55,000 Oe.

PREPARATION OF SAMPLES

The SMAD reactor for the preparation of Fe-based bimetallic materials has been described earlier *(26)*. Although several metals were coevaporated in this research, the evaporations all were carried out as follows.

Prior to the evaporation, approx 40–50 mL of pentane was first deposited on the walls of the reactor followed by the stepwise warm-up of the crucibles. The evaporation of iron was initiated after a steady evaporation of the second metal was achieved. The heating of iron was carefully controlled by slowly increasing the voltage to the crucible to prevent pressure surges in the reactor. In the whole evaporation process, a constant evaporation of the second metal and a constant deposition of pentane at a rate of 2–3 mL/min were ensured prior, during, and after

the iron evaporation. About 1 g of iron was evaporated in each experiment and about 100 mL of pentane was used. After the evaporation, an additional 40–50 mL of pentane was deposited to cover the product (about 200 mL total of liquid pentane).

After the final coating of pentane was finished, the reactor was closed off from the vacuum line. The liquid nitrogen dewar was removed to allow the reactor to warm to room temperature. Then the vacuum was reapplied to transfer the pentane to the cold trap and a black powder was obtained. The reactor was closed off from the vacuum line again and filled with argon to normal pressure. The lower part of the reactor containing the final product was quickly removed, covered with aluminum foil, and carefully transferred into an argon filled dry-box.

Heat treatments at various temperatures were applied to the collected particles to increase the sizes of the Fe crystallites within these particles. A certain amount of the sample, usually 70–100 mg, was transferred into a Pyrex glass tube in the argon-filled dry-box, then the glass tube filled with argon was sealed on a hydrogen/oxygen flame. After the sample was heated at the desired temperature over the desired time period, the sample tube was cut open in the dry-box and stored in a sample vial.

After the bimetallic powders were heat-treated, carefully controlled exposure to air (oxygen) was required to stabilize the surfaces of these particles against further oxidation (passivation). In the study of the Fe-Mg bimetallic materials, we experimented with three passivation procedures: slow oxidation, rapid oxidation, and combustion. It was concluded that only the slow exposure procedure could yield a controllable and reproducible result. Thus, only this passivation method was used for the samples in this part of the research, as described as follows.

A sample vial containing 50–100 mg of the fresh SMAD samples (heat-treated or as-prepared) was transferred from the dry-box into open air. The cap was then slightly opened to allow slow diffusion of air into the vial. After a 12–24-h period, the cap was removed and the sample was found to be stable against further oxidation. In some cases, the color of the sample changed slightly during this process.

RESULTS

The major thrust of this research was to employ a second metal (*M*) as a protecting reagent for small iron particles. Although no stable Fe-*M* alloys can be obtained from molten iron and the second metal, *M*, a low temperature bonding between Fe and *M* should be expected. This will enable the formation of a metastable amorphous Fe-*M* alloy through the coevaporation-deposition process, which may be explained by taking the Fe-Mg system as an example. Thermodynamically the formation of a homogeneous Fe-based alloy, such as Fe-Mg alloy requires a stronger Fe-

Mg interaction than those of Fe-Fe and Mg-Mg. Although until now no literature reports can be found on the comparison of these interactions, it is not very difficult to predict that in the Fe-Mg binary system, the Fe-Mg bonding is thermodynamically less favored, as evidenced by their immiscibility under normal conditions. In the low temperature deposition process, the mobility of the metal atoms is low. When a Fe-Mg bond is formed, it is unlikely to dissociate in the low temperature matrix. Therefore, a nonequilibrium amorphous Fe-Mg alloy can be obtained.

When heat is applied to these metastable amorphous Fe-based alloy particles, the mobility of metal atoms is greatly enhanced, and the energy provided will cause dissociation of Fe-*M* bonding and allow metal atoms to interact with each other to form thermodynamically more favored Fe-Fe and *M*-*M* bonds. When the temperatures increase, more Fe atoms will find each other to form larger Fe crystallites, and the original amorphous Fe-*M* alloy will be transformed into a two-phased structure with Fe crystallites as one phase and *M* metal as the second phase. However, the preferred structure, which can be described as a core/shell structure with Fe as the core, and the second metal *M* as the protecting shell, may not necessarily be achieved by the heating process. Based on common sense, we can assume that the formation of such a structure depends on many factors that can play a role in the segregation process, such as densities of the two metals, their melting points, surface tensions, and the bonding strengths between the metal atoms (Fe-*M*, *M*-*M*, and Fe-Fe).

The Iron–Indium System

A comparison of the basic properties of iron and indium is given in Table 1. The phase relationships in the Fe-In system can be characterized by a range of liquid immiscibility (3.4–91 at.%), the absence of compounds, and a low mutual solid solubility of Fe in liquid In, which only picks up when the temperature exceeds 800°C. Equilibrium temperatures of 800, 900, 1000, 1100, 1200, and 1300°C correspond to compositions of 0.27, 0.51, 1.0, 1.83, 3.53, and 5.98 at.% Fe *(29,30)*.

In our initial studies, a sample was prepared with an Fe:In molar ratio of 1:1, for which about 2.6 g of In and 1.3 g of Fe were coevaporated in the presence of pentane. After the evaporation, about 3 g of dark powder was collected from the reactor. XRD of the as-prepared sample showed a weak signal for indium, whereas no crystalline form of iron could be detected. A second Fe-In sample, with an Fe:In molar ratio of 2:1, was also studied. XRD of the as-prepared sample of this ratio showed iron and indium, both being nearly amorphous. Since the purpose of this experiment is to use indium metal to protect iron from oxidation, beyond the formation of a nearly homogeneous Fe-In amorphous alloy, it was considered desirable to have indium equal to Fe or in excess. Therefore, work was done most extensively with the 1:1 ratio.

Table 1
Properties of Iron and Indium

	Units	Iron (α-Fe)	Indium
Density	g/cm^3	7.87	7.31
Melting point	K	1808	429.6
Boiling point	K	3023	2285
Crystal structure	—	bcc	tetr
Electronegativity[a]	—	1.83	1.7
Valency	—	2,3,4	2 or 3

[a]Pauling electronegativity.

The as-prepared sample of the Fe:In = 1:1 system was divided into several portions and transferred into Pyrex glass tubes. All this was done in an atmosphere of argon. After these tubes were sealed, they were heated in a tube furnace at 200, 300, 350, or 400°C for 2 h, then the powders were transferred into small vials, slowly passivated, and analyzed by XRD. In the sample heated at 200°C, a strong In signal was detected, whereas only a weak Fe signal could be seen. Although no clear signs of either iron oxides or indium oxides were present, a small peak at 2θ of 41.5° suggested the presence of α-Fe_2O_3. After being heated at 300°C, the sample showed signals for Fe, In, α-Fe_2O_3, and In_2O_3. For the 350°C sample, a similar pattern was disclosed. In the 300 and 350°C samples, the In signals and the signals of indium oxide were about of the same strength.

After the sample had been heated at 400°C, the peaks of iron became much sharper, the signals of indium oxide also appeared stronger than in the samples heat-treated at lower temperatures (Fig. 2A), and there was still a weak peak for α-Fe_2O_3 at about 41.5° of 2θ. After these particles had been heated at 600 and 700°C, no iron oxide signals could be found even after extended exposure to air (Fig. 2B, C). In the Fe-In = 2:1 system, XRD results of the heat-treated samples showed similar results.

Since Fe and In are both susceptible to oxidation, the above XRD results suggest that when the heat treatment temperature gets high, more Fe atoms are driven into the center of the particles and are protected, whereas more In atoms are moved to the surfaces of the particles. During this process, the In reduces the iron oxides as well as scavenges any adventitious oxygen traces that might have been present. XRD and TEM studies gave the overall sizes and Fe crystallite sizes of these core/shell particles. These results are summarized in Table 2 and Fig. 3.

A room temperature Mössbauer spectrum of the Fe/In (2:1) particles is shown in Fig. 4. After the particles were heated at 400°C, the iron in the sample was much better protected and only a small amount of it was oxidized.

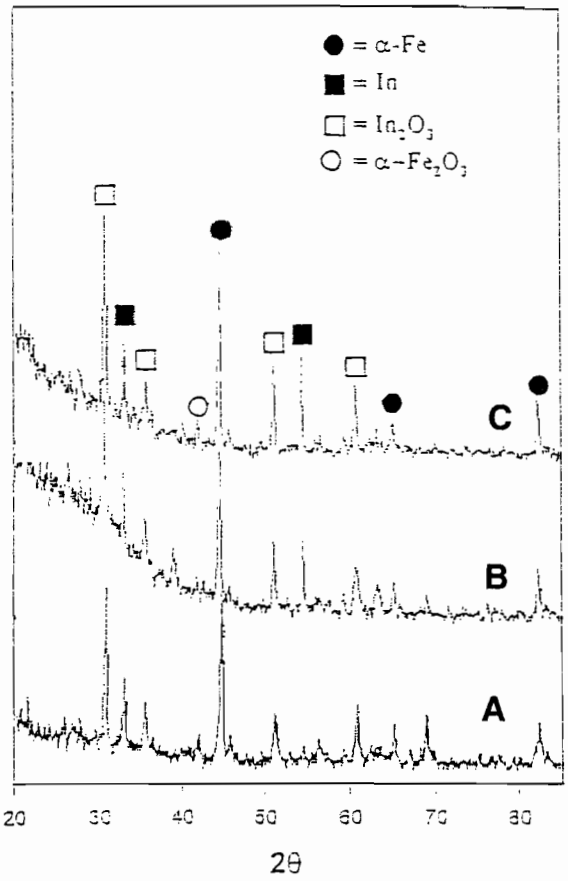

Fig. 2. XRD patterns of Fe-In SMAD particles (Fe:In = 1:1) heat-treated at **(A)** 400°C, **(B)** 600°C, and **(C)** 700°C for 2 h followed by oxidative passivation.

Table 2
Overall Particle Sizes and Fe Crystallite Sizes of Fe-In SMAD Particles Obtained from TEM and XRD Studies

Sample molar ratio, Fe:In	Heat treatment temperature, °C	TEM particle size, nm	XRD Fe crystallite size, nm
1:1	Fresh, not heated	—	3
1:1	200	12	7
1:1	300	23	16
1:1	350	30	21
1:1	400	70	31
2:1	Fresh, not heated	—	4
2:1	200	20	7
2:1	300	30	11
2:1	400	80	29

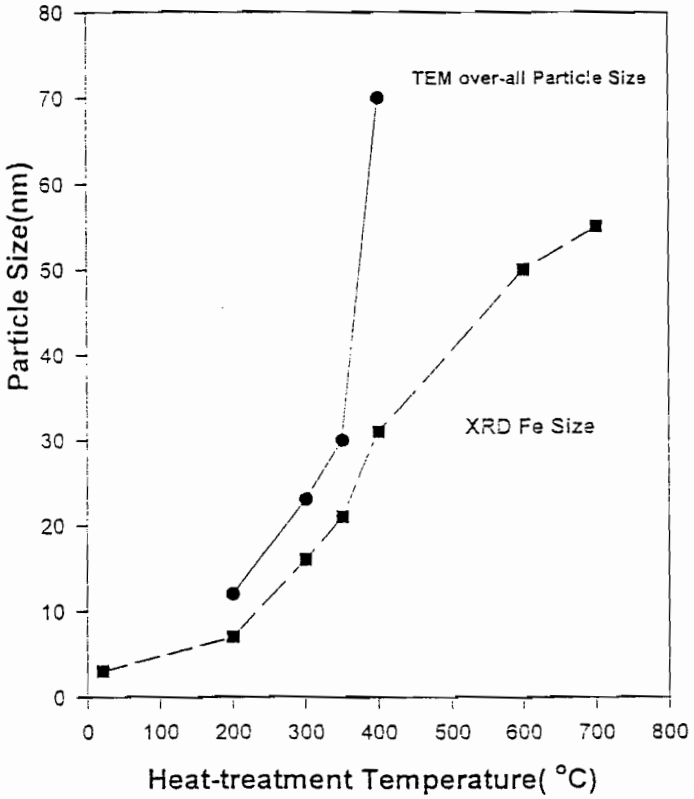

Fig. 3. XRD Fe crystallite sizes and TEM overall particle sizes of Fe-In samples with an Fe:In molar ratio of 1:1.

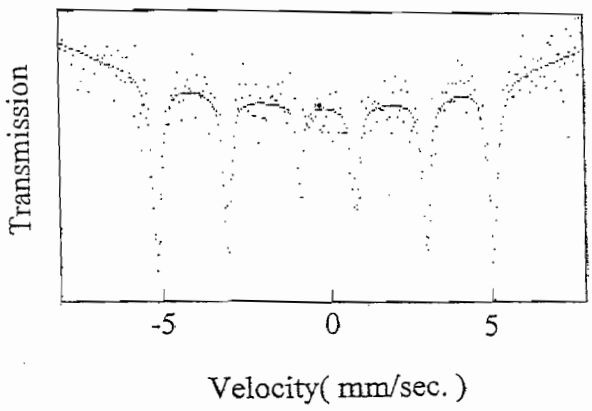

Fig. 4. Room temperature Mössbauer spectrum of Fe-In (Fe:In = 2:1) SMAD particles heat-treated at 400°C followed by oxidative passivation.

Table 3
Saturation Magnetization Values (emu/g of Iron) for Samples with Fe:In Molar Ratios of 1:1 and 2:1 at 10, 150, and 300K

Sample Fe:In ratio/heat-treatment temperature	Fe XRD size, nm	10K	150K	300K
1:1/fresh, not heated	3	99	89	74
1:1/200°C	7	104	102	98
1:1/300°C	16	115	113	110
1:1/350°C	21	119	117	113
1:1/400°C	31	150	148	145
1:1/600°C	50	214	211	206
1:1/700°C	55	213	209	207
2:1/fresh, not heated	4	163	155	140
2:1/200°C	7	152	148	145
2:1/300°C	11	172	170	167
2:1/400°C	29	192	189	187
2:1/600°C	50	221	216	213
2:1/700°C	60	219	215	212

The magnetic properties of these samples were obtained on a SQUID magnetometer. In a mixture of Fe/In/α-Fe_2O_3/In_2O_3, only Fe is strongly magnetic with a saturation magnetization value of 220 emu/g, whereas α-Fe_2O_3 is only slightly magnetic with a saturation magnetization value of 0.6 emu/g and neither In nor In_2O_3 is magnetic. Since SQUID can only provide the overall magnetization value of the sample, it is necessary to translate the SQUID data into the magnetization values of metallic iron. If the samples did not take up any oxygen during the passivation process, the chemical compositions of these samples would be very close to those of the starting materials. For example, for the Fe:In = 1:1 system, this will be Fe 33% by mass and In 67% by mass. Based on XRD and Mössbauer data, it can be estimated that on average about 50% of the In is in the form of In_2O_3 after our passivation procedure. This translates into a mass balance for Fe° for the Fe:In = 1:1 system of 30%. For the Fe:In = 2:1 system, the Fe° mass balance would be 46%. These values were used in calculation of the saturation magnetization per gram of iron values (emu/g of Fe), and they are shown in Table 3. The coercivity values are shown in Table 4, whereas Fig. 5 plots the M_S values vs Fe° crystallite sizes.

The Iron-Neodymium System

Recall that an Fe-Nd-B alloy is the strongest permanent magnet material known *(31)* but little is known about the magnetic properties of Fe-Nd-B small particles. As a starting point, it is believed that a study of the properties of Fe-Nd particles would be of some interest. The binary

Table 4
Coercivity Values in Oersteds of Fe-In Samples at Different Temperatures

Sample Fe:In ratio/treatment temperature (°C)	10K	77K	150K	220K	300K
1:1/200	250	100	60	45	20
1:1/300	235	100	75	40	30
1:1/350	50	35	20	20	10
1:1/400	35	17	20	140	100
1:1/600	10	5	5	5	5
2:1/200	145	120	110	100	105
2:1/300	150	113	105	105	105
2:1/400	85	55	35	50	30
1:1/fresh, not heated	5	10	27	48	190
2:1/fresh, not heated	300	175	107	75	45

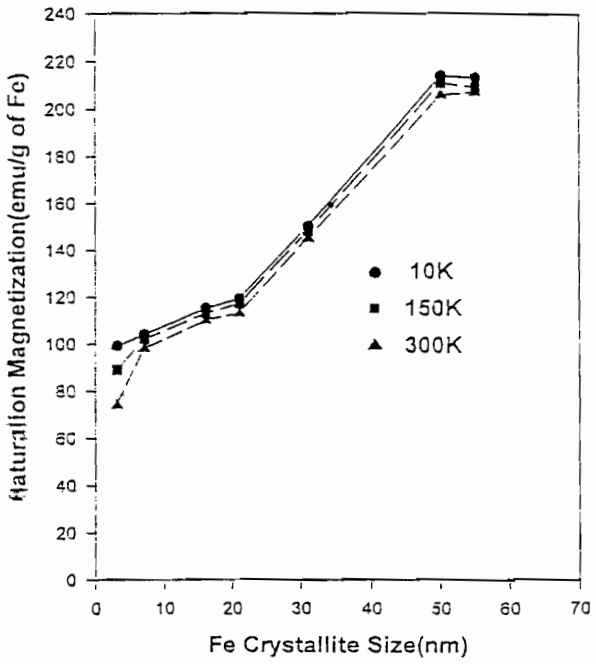

Fig. 5. Saturation magnetization values of Fe-In (Fe:In = 1:1 samples vs different Fe crystallite sizes in these particles.

phase diagram of the Fe-Nd system shows a miscible system with two stable compounds $Fe_{17}Nd_2$ and Fe_2Nd (*32*). However, when Nd is used in excess, it may still form a protective coating. Also, since the SMAD

method is a very different process for the formation of Fe-Nd compounds compared with the conventional melting method, it was not known if Fe and Nd would form compounds after they were coevaporated in the SMAD reactor and underwent heat treatments under relatively mild temperatures.

Evaporation of the two metals was carried out in the same SMAD reactor. Fe was evaporated out of an alumina-coated tungsten crucible and Nd from a boron nitride crucible placed in a tungsten basket with alumina coating on the outside. Pentane was used as the organic solvent. Several reactions were carried out using a molar ratio of Fe/Nd of 1:1. In a typical reaction in which about 0.56 g of Fe (10.0 mmol) and 1.5 g of Nd (10.4 mmol) were used, 1.6 g of black pyrophoric powder was collected. Elemental analysis of the powder gave 25.1 and 69.3% by weight Fe and Nd, respectively *(33)*.

The pyrophoric fresh Fe-Nd powders were then heat-treated under argon at different temperatures ranging from 250 to 750°C for 2 h. After the heat treatments, these powders were slowly passivated in air, allowing a layer of metal oxides to form on the surfaces of these powders. No evident physical changes were observed for the stabilized powders after they had been stored in sample vials for 6 mos.

An XRD pattern of the fresh Fe-Nd pentane SMAD powder showed only one broad peak because of metallic iron. The XRD patterns of heat-treated and passivated powders showed that the iron began to crystallize at a very low temperature (Fig. 6), but clear signals for Nd_2O_3 were not observed until the heat treatment temperature reached 500°C. In addition, no clear signals for iron oxides or metallic Nd could be seen through all the heat treatment experiments. A weak signal for the Fe-Nd intermetallic compound Fe_2Nd was observed for samples heated at 500°C and above. The average XRD α-Fe crystallite sizes, estimated with the Sherrer formula, are listed in Table 5 along with the BET surface area data and the estimated sample densities. The BET overall particle sizes listed in this table were estimated from the BET surface area data and the sample densities, assuming all the particles have a spherical shape. For comparison, the estimated TEM sizes of these particles are also listed in Table 5.

To determine the valence states of Fe atoms in these samples, Mössbauer spectra were taken. When exposed to air, all the Fe atoms in the as-prepared particles were oxidized to α-Fe_2O_3. The heat-treated and passivated Fe-Nd samples showed a gradual increase of the percentage of metallic Fe (as the α-Fe sextet) on increase of the heat treatment temperature. These changes, together with the Mössbauer data on the metallic α-Fe phase (sextet) in these powders, are summarized in Table 6. The Mössbauer data indicated the presence of pure α-Fe, whereas the rest of the signal can be assigned to α-Fe_2O_3 and Fe_2Nd. Since the signals of α-Fe_2O_3 and Fe_2Nd (each as a doublet) overlap with each other, we could not assess their relative abundance.

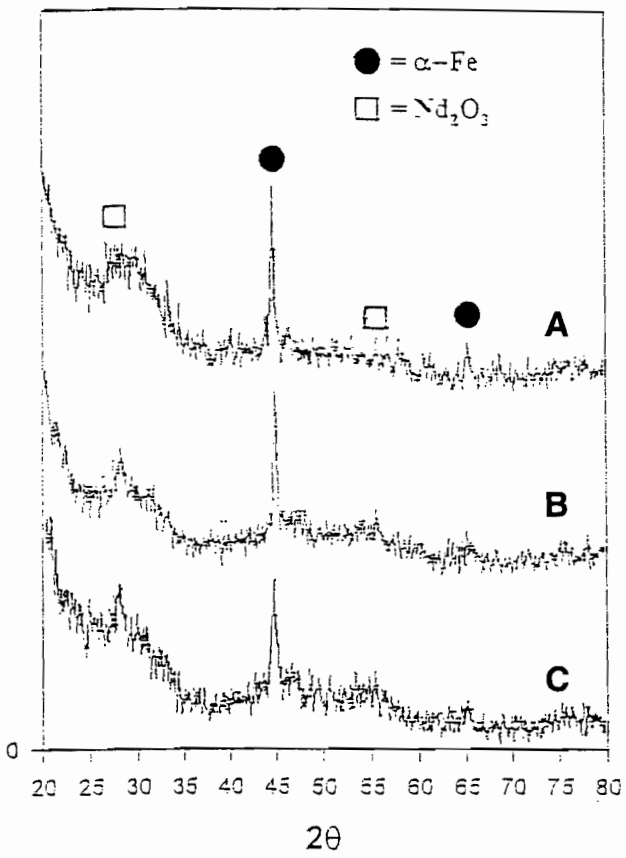

Fig. 6. XRD patterns of heat-treated and passivated Fe-Nd particles: **(A)** T = 450°C; **(B)** T = 325°C; **(C)** T = 225°C.

The hyperfine field of the fresh, unexposed Fe-Nd powder (324 KOe) is slightly lower than the standard value (333 KOe). This may indicate a close-range electronic interaction between iron (electronegativity 1.8) and Nd (electronegativity 1.1) atoms that enables Fe atoms to withdraw some electron density from the surrounding Nd atoms.

The Mössbauer data showed that when the samples were heat-treated at temperatures higher than 450°C, at least 70% of the iron atoms were protected from further oxidation (as α-Fe) after the powders were stabilized by oxidative passivation of the surfaces. However, a Mössbauer spectrum of the sample heat-treated at 750°C showed a slightly lower content of the α-Fe phase. This may be because more Fe atoms formed Fe_2Nd at this high temperature. Also, the extensive sintering of the surface layer may lead to the exposure of the Fe crystallites to oxygen (the protecting shell may shrink and expose the α-Fe core to oxygen).

Magnetic studies of these Fe-Nd bimetallic particles allowed us to examine the saturation magnetization and coercivity values of these

Table 5
XRD, TEM Sizes, and BET Surface Area Data on Fe-Nd (Fe:Nd = 1:1) Samples

Sample	TEM size, nm	XRD Fe size, nm	BET size, nm[a]	BET specific surface area, m^2/g	Density, g/cm^3[b]
Fresh, not heated	—	2–3	93	8.7	7.4
Heated at 225°C and passivated	12	8	32	28	6.8
Heated at 325°C and passivated	—	14	29	30	6.9
Heated at 450°C and passivated	—	19	25	34	7.1
Heated at 600°C and passivated	30	26	—	—	7.2
Heated at 750°C and passivated	35	29	25	34	7.1

[a]Assuming all the particles had a spherical shape.
[b]Estimation was based on the information obtained from XRD and Mössbauer studies on the concentrations of Fe, α-Fe_2O_3, and Nd_2O_3.

Table 6
Room Temperature Mössbauer Data on Fe-Nd Samples

Sample heat treatment temperature, °C	Isomer shift (IS), mm/s	Quadrupole splitting (OS) mm/s	Hyperfine field (H), KOe	% of Fe as α-Fe sextet
Fresh, not heated	–0.01	0.02	323.2	—
225°C, passivated	0.02	0.04	332.8	54
325°C, passivated	–0.01	–0.03	332.7	59
450°C, passivated	0.06	0.09	329.6	71
500°C, passivated	–0.01	–0.01	332.1	70
600°C, passivated	0.06	0.04	330.5	74
750°C, passivated	–0.02	–0.02	333.1	68
Not heated, passivated (mainly α-Fe_2O_3, a doublet)	0.24	0.96	—	0–10

powders. Based on the XRD patterns, it can be concluded that none of the exposed samples had metallic Nd as a component. This made it possible to assign all Nd as Nd_2O_3 in all the exposed particles, and all the Fe atoms were considered as metallic Fe when the mass balance of the passivated samples was calculated. This gave an estimated Fe mass balance of 25% for all the passivated samples with starting Fe/Nd molar

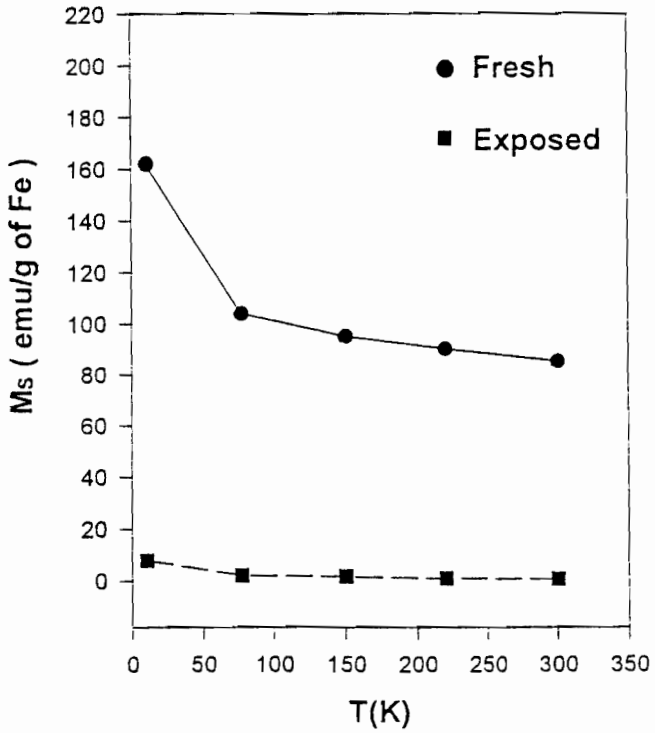

Fig. 7. Saturation magnetization values of fresh and exposed Fe-Nd particles (neither heat-treated).

ratio of 1:1. For fresh, unexposed Fe-Nd bimetallic powders, only metallic Fe atoms and metallic Nd atoms were considered as the components, and for the Fe:Nd = 1:1 system, the theoretical mass balance for Fe was about 28%. The comparison between the saturation magnetization values of the fresh, unexposed Fe-Nd sample (not heated) and the as-prepared, exposed Fe-Nd sample (not heated) is illustrated in Fig. 7, and the comparison of their coercivities is given in Fig. 8. From Fig. 7 it is noted that the saturation magnetization value of the fresh, as-prepared Fe-Nd sample has a strong temperature dependence. It was about 162 emu/g of Fe at 10K, and gradually decreased to about 85 emu/g of Fe at 300K. Since there was no oxygen in this sample, the lower M_s values of this sample compared with that of the bulk Fe was probably caused by the formation of Fe-Nd alloys on the surfaces of the iron crystallites; this surface effect will be discussed later. The exposed Fe-Nd particles (not heated) had very low M_s values, which confirmed that most of the iron atoms in this sample were oxidized to α-Fe_2O_3 during the exposure to air, as indicated by the room temperature Mössbauer data. The coercivity values of the fresh and exposed particles are also quite different. The high coercivities of the fresh, as-prepared Fe-Nd particles indicate that this sample con-

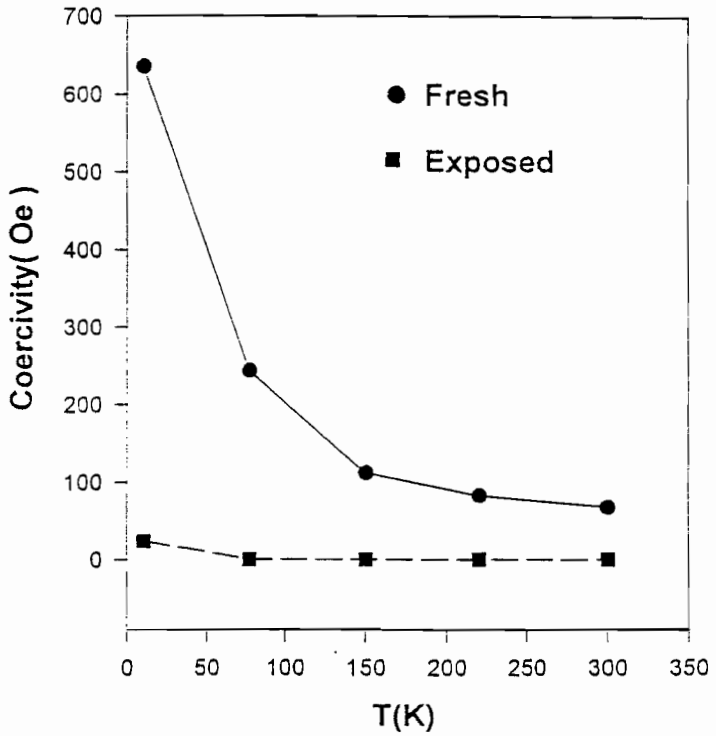

Fig. 8. Coercivities of fresh and exposed Fe-Nd particles (neither heat-treated).

tains ferromagnetic metallic iron clusters, whereas that very low coercivities of the exposed Fe-Nd sample are a result of amorphous α-Fe_2O_3 (Fig. 8).

Although no information on the magnetic properties of Nd_2O_3 was found in the literature, it is reasonable to believe that Nd_2O_3 has a very low magnetic moment. Therefore, we can omit the contribution of Nd_2O_3 to the saturation magnetization values of the passivated Fe-Nd particles. Furthermore, we know α-Fe_2O_3 has a saturation magnetization value of 0.6 emu/g, compared to the saturation magnetization value of pure Fe at 220 emu/g, so it is believed that the magnetic moment of these samples comes only from metallic Fe. Based on the estimated mass balance of these samples, the magnetization values of the passivated Fe-Nd particles were calculated and are illustrated in Fig. 9 vs the Fe crystallite sizes.

Note that passivated Fe-Nd particles have reduced saturation magnetization values, which is because of oxidation on passivation, especially of the unheat-treated samples. However, the formation of Fe-Nd alloys on the surfaces of the Fe clusters should also be taken into consideration. For samples heated at lower temperatures (small Fe crystallites), the oxidation effect probably predominates, whereas for samples

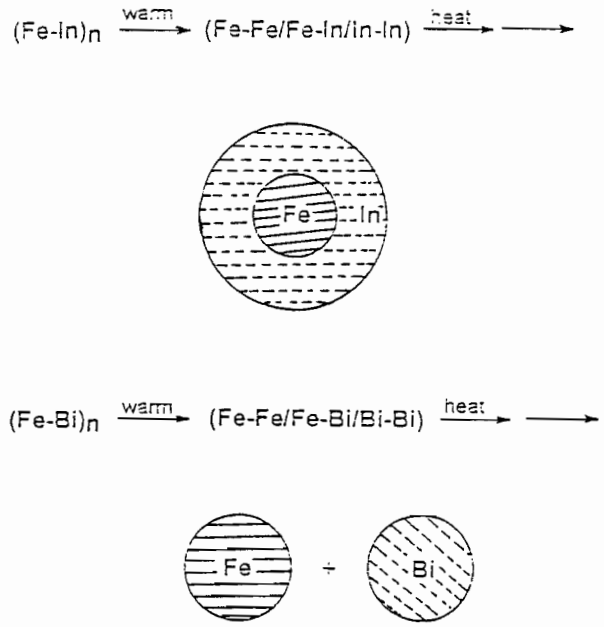

Fig. 9. Phase segregation in Fe-In and Fe-Bi nanoscale particles.

heated at higher temperatures, less Fe was oxidized and more Fe would form alloys with Nd. The low M_s value of the 750°C sample (compared with the 600°C sample) is possibly because of the extensive formation of Fe_2Nd in this sample.

The coercivities of the passivated Fe-Nd particles were very low, between 12.6 and 105 Oe at 300K. For α-Fe crystallites with an iron oxide outside coating, room-temperature coercivity values can be as high as 1050 Oe *(34)*; thus, these Fe-Nd powders must be considered soft magnetic materials and consist of Fe° clusters protected by Fe_2Nd and Nd_2O_3 coatings.

Other Systems

Iron-Gold System

Considering the phase diagram of the Fe-Au system, there are no intermetallic compounds, and Fe and Au are immiscible below 475°C *(35)*. At 500°C, the solid solubility of gold in iron is between 0.1 and 0.14, whereas the maximum solubility of Au in α-Fe is 2.3 at.% Au at 903°C *(35,36)*. The immiscibility of the Fe-Au system at low temperature and the low miscibility of these components at high temperatures makes it a possible candidate for the preparation of protected Fe crystallites with the SMAD method. For the SMAD Fe-Au evaporation, several Fe:Au atomic ratios were selected. They are Fe:Au = 1:2, 1:1, 2:1, and 3:1. The XRD patterns of the Fe:Au = 2:1 and Fe:Au = 3:1 samples showed only

Table 7
Magnetization Values of Passivated Fe-Au Particles Measured at Temperatures Ranging from 10–300K

Sample molar ratio and heat treatment temperature	10K	77K	150K	220K	300K
Fe:Au = 1:2, 400°C	122[a]	131	124	118	109
Fe:Au = 1:1, 400°C	75.3	71.3	67.5	64.2	59.0
Fe:Au = 2:1, 400°C	20.0	18.9	16.5	14.2	13.0
Fe:Au = 3:1, 250°C	11.2	10.2	8.2	7.6	5.0
Fe:Au = 3:1, 400°C	17.5	15.3	13.0	11.3	9.0

[a]All values are in emu/g of Fe.

the signals for Au. This suggests that Fe is in an amorphous state in these as-prepared Fe-Au samples. Mössbauer spectroscopy was also employed to study these particles, but only a single broad absorption was found. This is possibly because of the shielding effect of gold on the γ-rays. After being heat-treated at temperatures up to 400°C, these materials still gave no clear Mössbauer signals. Besides the possible shielding effect of gold, another possible reason for this is that Fe remained in an amorphous state even after these heat treatment procedures. The magnetic properties of these materials are listed in Table 7. The magnetization values of the passivated Fe-Au particles at 300K showed that for the Fe:Au = 2:1 system, about 50% of the Fe remained in the metallic state. Only about 25% of the Fe was protected in the Fe:Au = 1:1 system. For the Fe:Au = 2:1 and 3:1 system, almost all of the Fe was oxidized when the samples were exposed to air. The aforementioned results lead to the conclusion that the Fe-Au system does not behave in the desired way, and the heating/phase segregation process leads to a mixture of separated (unprotected) Fe and Au particles. Similar results were found for the Fe-Ag system *(37)*.

Fe-Bi, Fe-Ca, Co-Mg, and Ni-Mg Systems

The Fe-Bi combination is also immiscible. Stable intermetallic phases in the Fe-Bi system do not form and mutual solubilities in the liquid and solid states are very low *(38)*. The XRD patterns of the SMAD as-prepared Fe-Bi particles showed only strong signals of bismuth. The XRD pattern of the Fe-Bi powder, heated at 300°C and then passivated, showed only bismuth and Fe_2O_3. The Mössbauer spectrum of the Fe-Bi particles heated at 400°C followed by passivation also showed no indication of the presence of metallic iron. Thus, like Fe-Au, the Fe-Bi system is also unfavorable for our purpose. Bismuth did not serve as a good protecting agent for the Fe elements in the Fe-Bi mixture.

The workability of Fe-Ca, Co-Mg, and Ni-Mg systems were also explored. The oxidation behavior of Ca is very complex. Furthermore, the resulted calcium oxides were very hygroscopic. All this made the characterization highly difficult, and the Fe crystallites in these materials were found not to be well protected. The Co-Mg and Ni-Mg systems are miscible binary systems. Stable Co-Mg and Ni-Mg intermetallic compounds were formed in the SMAD preparation of these samples, and so the desired core/shell morphologies were not produced.

DISCUSSION

The SMAD method can be utilized to prepare nanoparticulate metastable alloys of two normally immiscible metals. On heat treatment of these $(M\text{-}M')_n$ particles, phase segregation occurs. In the case of Fe-Mg, Fe-In, and Fe-Nd, the phase segregation leads to core/shell structures where Fe is the core. In the case of Fe-Au, Fe-Ag, and Fe-Bi, phase separation did not lead to core/shell structure, but instead individual particles of the two metals. The core/shell structure formation is apparently controlled by metal-metal bond strengths, as well as surface tension and wetting. For example, in the Fe-In system, Fe-Fe bonds are stronger than In-In or In-Fe, and so on heating, as the atoms become mobile, Fe atoms "find each other;" they remain bound, whereas Fe-In and In-In bond formations are less robust, eventually leading to Fe cluster formation. It is also necessary that the surface wetting of the Fe clusters by the In coating be energetically favorable, which apparently is the case with Mg, In, and Nd, but not with Ag, Au, and Bi, as shown in Fig. 9.

When the core/shell structure forms, excellent protection of the Fe clusters results, and exposure to the environment is not detrimental. The heat treatment temperature controls the ultimate Fe cluster sizes. If the temperature is too low, sometimes complete oxidative protection is not achieved. However, heat treatments of 500–600°C with the Fe-In and Fe-Nd systems yielded protected $[M]_{coating}[Fe]_{core}$ structures. Under these conditions the sizes of the Fe crystallites were 50–55 nm for Fe-In and 30–35 nm for Fe-Nd, and they exhibited saturation magnetization values close to the bulk value of iron metal. However, smaller crystallites (low heat treatment temperature) gave values considerably lower than the bulk value, and M_s increased with crystallite size (Fig. 5 and Fig. 10). We believe this is at least partially the result of a "dead-layer effect," in which the Fe surface atoms are deadened by the In or Nd interface. Since smaller particles have higher ratios of surface atoms/total atoms, this deadening effect would become more predominant with decrease in Fe crystallite sizes. Unfortunately, partial oxidation of the iron also may have contributed to this lowering of M_s, especially in the unheated samples, so quantitative studies can only be done on absolutely pristine samples; these studies will be reported soon.

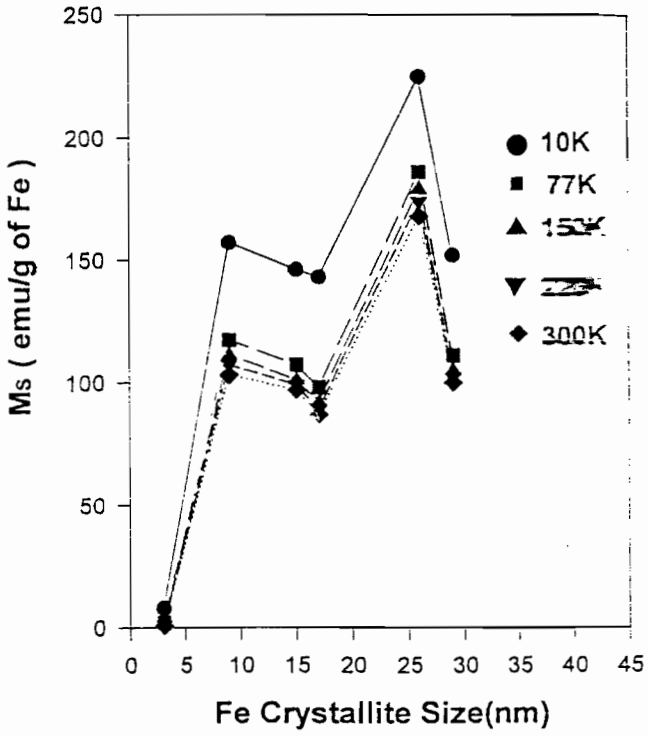

Fig. 10. Saturation magnetization values of passivated Fe-Nd particles with different Fe crystallite sizes.

Another interesting feature of the core/shell Fe-In and Fe-Nd samples is their very low coercivities, which was also found for similar Fe-Mg samples *(28)*. They are all soft magnetic materials, which suggests that Mg, In, and Nd coatings do not hinder the magnetic field switching. To summarize what has been accomplished: Gram quantities of core/shell nanoparticles of iron metal powders have been synthesized, where the shell material protects the iron from oxidation.

ACKNOWLEDGMENT

The support of the National Science Foundation is acknowledged with gratitude.

REFERENCES

1. Sharrock, M. P. and Bodnar, R. E., *J. Appl. Phys.* **57,** (1985)
2. Sharrock, M. P., *MRS Bull.* Vol. XV, **53,** (1990).
3. Sharrock, M. P., *IEEE Trans. Magn.* **26,** 193, (1990).
4. Tasaki, A., Saegusa, N., and Oda, M., *IEEE Trans. Magn.* Vol. MAG-19, No.5, **1731,** (1983).
5. Gleiter, H., *Prog. Mater. Sci.* **33,** 223, (1989).

6. Jen, S. U., Lee, C. Y., Yao, Y. D., and Lee, K. C., *J. Magn. Mater.* **96,** 82, (1991).
7. Baldokhin, Yu. V., Kolotyrkin, P. Ya., Petrov, Yu. I., and Shafranovsky, E. A., *J. Appl. Phys.* **76,** 6496, 1994. (1994).
8. Dragieva, I., Gavrilov, G., Buchkov, D., and Slavcheva, M., *J. Less-Common Met.* **67,** 375, (1979).
9a. Corrias, A., Ennas, G., Licheri, G., Marongiu, G., and Paschina, G., *Chem. Mater.* **2,** 363, (1990).
9b. Glavee, G. N., Klabunde, K. J., Sorensen, C. S., and Hadjipanayis, G. C., *Inorg. Chem.* **32,** 474, (1993).
10. Rieke, R. D., *Acc. Chem. Res.* **10,** 301, (1977).
11. Rochfort, G. L. and Rieke, R. D., *Inorg. Chem.* **25,** 348, (1986).
12. Bönnemann, H., Brijoux, W., and Joussen, T., *Angew. Chem. Int. Ed. Engl.* **29,** 273, (1990).
13. Nagashima, K., Wada, M., and Kato, A., *J. Mater. Res.* **5,** 2828, (1990).
14. Suslick, K. S., Choe, S.-B., Cichowlas, A. A., and Grinstaff, M. W., *Nature,* **353,** 414, (1991).
15. Chen, J. P., Sorensen, C. M., Klabunde, K. J., and Hadjipanayis, G. C., *Phys. Rev. B* **51,** 527, (1995).
16. Rivas, J., López-Quintela, M. A., López-Pérez, J. A., Liz, L., and Duro, R. J., *IEEE Trans. Magn.* **29,** 2665, (1993).
17. Oku, T., Sato, T., and Ohta, E., *J. Magn. Mater.* **116–117,** 148, (1995).
18. Dormann, J. L., Sella, C., Renaudin, P., and Gibart, P., *Thin Solid Films* **5,** 983, (1979).
19. Papaefthymiou, V., Tsoukatos, A., Hadjipanayis, G. C., Simpoulos, A., and Kostikas, A., *J. Magn. Mater.* **140–144,** 397, (1995).
20. Kawaguchi, K., Yamamato, R., Hosoito, N., Shinjo, T., and Takada, T., *J. Phys. Soc. Jpn.* **55,** 2375, (1986).
21. Giri, A. K., de Julián, C., and Gonzaléz, J. M., *J. Appl. Phys.* **46,** 6573, (1994).
22. Kuhrt, C.; Schultz, L. *IEEE Trans. Magn.* **29(6),** 2667 (1993).
23. Buschow, K. H. J. and van der Kraan, A. M. *Phys. Stat. Sol. (a)* **53,** 665, (1979).
24. Buschow, K. H. J. and van der Kraan, A. M. *J. Magn. Mater.* **22,** 220, (1981).
25. Hickey, B. J., Howson, M. A., Musa, S. D., and Wiser, N. *Phys. Rev. B.* **51,** 667, (1995).
26a. Klabunde, K. J., Efner, H. F., Murdock, T. O., and Ropple, R. *J. Am. Chem. Soc.* **98,** 1021, (1976).
26b. Klabunde, K. J., *Free Atoms, Clusters, and Nanoscale Particles*; Academic, San Diego, CA, 1994.
26c. Klabunde K. J. and Cardenas-Trivino, G., in *Active Metals—Preparation, Characterization, Applications*, (Fürstner, A., ed.), VCH, Weinheim, 1996, pp. 237.
27. Glavee, G. N., Kernizan, C. F., Klabunde, K. J., Sorensen, C. M., and Hadjipanayis, G. C., *Chem. Mater.* **3,** 967, (1991).
28. Klabunde, K. J., Zhang, D., Glavee, G. N., Sorensen, C. M., and Hadjipanayis, G. C., *Chem. Mater.* **6,** 784, (1994).
29. in *Binary Alloy Phase Diagrams*, (Massalski, T. B., Murray, J. L., Bennett, L. H., Baker, H., and Kacprzak, L., eds.), American Society For Metals, 1986, vol. I, pp. 1071.
30. Kubaschewski, O. *IRON-Binary Diagrams*; Phase Springer-Verlag: Berlin Heidelberg New York Verlag Stahleisen m.b.H. Düsseldorf, 1982, pp. 53–55.
31. Hadjipanayis, G. C., Hazelton, R. C., and Lawless, K. R., *J. Appl. Phys.* **55,** 2073, (1984).
32. in *Binary Alloy Phase Diagrams*, (Massalski, T. B., Murray, J. L., Bennett, L. H., Baker, H., and Kacprzak, L., eds.), American Society for Metals, 1986; vol. I, pp. 1085.
33. Elemental analysis results were obtained from Galbraith Laboratories, Inc.
34. Gangopadhyay, S., Hadjipanayis, G. C., Dale, B., Sorensen, C. M., Klabunde, K. J., Papaefthymiou, V., and Kostikas, A. *Phys. Rev.* B **45,** 9778, (1992).
35. in *Binary Alloy Phase Diagrams*, (Massalski, T. B., Murray, J. L., Bennett, L. H., Baker, H., and Kacprzak, L., eds.), American Society For Metals, 1986, vol. I, pp. 259.
36. Kubaschewski, O. *IRON-Binary Phase Diagrams*; Springer-Verlag: Berlin Heidelberg New York Verlag Stahleisen m b.H. Düsseldorf, 1982, pp. 13–15.
37. Easom, K. A., Klabunde, K. J., Sorensen, C. M., and Hadjipanayis, G. C., *Polyhedron* **13,** 1197, (1994).
38. Kubaschewski, O. *IRON-Binary Phase Diagrams*; Springer-Verlag: Berlin Heidelberg New York Verlag Stahleisen m.b.H. Düsseldorf, 1982; pp. 22.